Phonon scattering at a rough interface between two fcc lattices

Hong Zhao[1,a] and Jonathan B. Freund[1,2,b]
[1]*Department of Mechanical Science and Engineering, University of Illinois at Urbana-Champaign, 1206 West Green Street, Urbana, Illinois 61801, USA*
[2]*Department of Aerospace Engineering, University of Illinois at Urbana-Champaign, 104 South Wright Street, Urbana, Illinois 61801, USA*

(Received 25 August 2008; accepted 11 November 2008; published online 7 January 2009)

Elastic phonon scattering at an atomically rough interface that separates two fcc lattice leads is computed via a Green's function method. Results are compared to specular and diffuse phonon scattering models, both of which are widely used in the numerical simulations of phonon Boltzmann transport equations. The shape of the discrete interface in the model is quantified by its spectral characteristics. It is found that the amplitude of the interface height fluctuations has strong influence on the effective interface specularity, while the effect of the two-point correlation length is minor. The average phonon transmission coefficient as well as the overall thermal resistance, however, is relatively insensitive to the interface roughness. © *2009 American Institute of Physics*.
[DOI: 10.1063/1.3054383]

I. INTRODUCTION

For heat transfer in nanometer-scale semiconductor structures, a fundamental problem is phonon scattering at the interface between different materials. Interface reflections introduce a temperature jump proportional to the cross-plane heat flux, and their ratio is the so called thermal boundary resistance or Kapitza resistance.[1,2] For modeling tools such as the phonon Boltzmann transport equation (BTE), interfacial scattering is part of the boundary conditions.[3–5] In structures such as thin films, whose characteristic length scale is comparable to the phonon mean free path, the phonon transport is nearly ballistic and the interface scattering becomes the dominant mechanism of thermal resistance. Hence our prediction capability can be limited by models for phonon interface scattering. In this paper, we design a model for which it is possible to construct exact solutions in the linear limit, but general enough to permit complete flexibility in the nature of the atomic mixing in the neighborhood of the interface. Results provide a means of testing the simplified boundary conditions often used in BTE models.

A. The model system

We consider elastic phonon scattering at the junction between two fcc lattice leads, as shown in Fig. 1. The interface Γ is defined by a surface $x=h(y,z)$ such that atoms are of type 1 to the left of the interface and of type 2 to the right. The left and right lattice leads have the same lattice constant a. Each atom is identified by an integer triplet (i,j,k) of even sum $(i+j+k)$, which determines the atom's equilibrium position $\mathbf{R}_{ijk}=a/2(i,j,k)$. The system is periodic in the y and z directions, with periodicities $N_y a$ and $N_z a$. Thus the phonon scattering is caused by the mismatch in atomic mass and interactions, while other possible factors such as the mismatch in lattice constant and defects are not included.

The atomic interaction is modeled by a two-body potential that is nonzero only between nearest neighbor sites. The potential energy has harmonic approximation at small displacement

$$\phi[\mathbf{r}(\mathbf{R}),\mathbf{r}(\mathbf{R}')] \approx \frac{K}{2} \times [|\mathbf{r}(\mathbf{R}) - \mathbf{r}(\mathbf{R}')| - |\mathbf{R} - \mathbf{R}'|]^2 \tag{1}$$

$$\approx \frac{K}{2} \times \left(\frac{\mathbf{R} - \mathbf{R}'}{|\mathbf{R} - \mathbf{R}'|} \cdot [\mathbf{u}(\mathbf{R}) - \mathbf{u}(\mathbf{R}')] \right)^2, \tag{2}$$

where $\mathbf{r}(\mathbf{R})$ is the displaced (current) atomic position and $\mathbf{u}(\mathbf{R})=\mathbf{r}(\mathbf{R})-\mathbf{R}$ is the displacement. The force constant is $K=K_1$ when both atoms are of type 1, and $K=K_2$ when both atoms are of type 2. For interactions between two atoms of different types, we let $K=\sqrt{K_1 K_2}$. Quantities are nondimensionalized by the atomic mass M_1, spring constant K_1, and the lattice constant a. The phonon dispersions of the left and right lattice leads mimic those of the acoustic phonons in bulk silicon and germanium crystals, so we set $M_2/M_1=2.585$ and $K_2/K_1=0.888$ based on their atomic mass and the speeds of sound.[6]

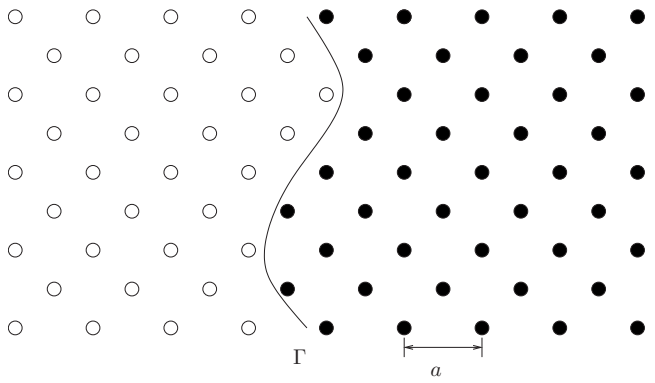

FIG. 1. The model composite fcc lattice showing the discrete atomic positions and equivalent continuum interface shape Γ.

[a]Electronic mail: hongzhao@uiuc.edu.
[b]Electronic mail: jbfreund@uiuc.edu.

B. Empirical scattering models

Two widely used phonon scattering models are the acoustic mismatch model (AMM) and the diffuse mismatch model (DMM).[2,7] The AMM is a low wavelength (or low frequency) limit, where the characteristic length scale of the interface roughness is assumed to be much smaller than the incoming phonon wavelength. In this regime, the scattering process can be approximated by that of acoustic waves at the junction between two macroscopic elastic leads. The simplest AMM model neglects the mode conversion between longitudinal and transverse phonon modes. Letting ρ be the material density and c be the speed of sound, the AMM prediction of the phonon transmission coefficient $\mathcal{T}$ from medium 1 to 2 is

$$\mathcal{T}_{1\to 2} = \frac{4Z_1Z_2}{(Z_1+Z_2)^2} \quad \text{with } Z_i = \frac{\rho_i c_i}{\cos\theta_i} \quad \text{and} \quad \frac{\sin\theta_1}{\sin\theta_2} = \frac{c_1}{c_2}, \tag{3}$$

where $\theta_{1,2}$ are the angles of incoming and transmission and $Z_{1,2}$ are the material acoustic impedances. A similar specular scattering model applies at a perfectly specular interface.[8,9] Since the composite lattice is discretely translationally invariant in transverse directions, a scattered phonon matches the same transverse wave numbers as the incoming phonon and the scattering problem can be solved analytically. In the low frequency limit, the specular scattering model of course reduces to AMM, but it deviates significantly with increasing frequencies because of the nonlinear and anisotropic phonon dispersion properties of any lattice.

In contrast to the AMM, the DMM represents a high frequency limit. The essential assumption is that the scattered phonon mode is completely uncorrelated to the incoming mode. Incoming phonons of the same frequency thus have the same transmissivity, which can be computed by the energy flow balance.[2] For the system in Fig. 1 that is finite in the y-z plane, the DMM predicts

$$\mathcal{T}_{1\to 2} = 1 - \mathcal{T}_{2\to 1} = \frac{N_2}{N_1+N_2}, \tag{4}$$

where $N_{1,2}$ are the numbers of discrete incoming phonon modes at the given frequency. Under the Debye approximation,[10] phonon modes of branch s ($s=1,2,3$) at a low frequency ω on side i ($i=1,2$) have

$$|\mathbf{q}|^2 = q_x^2 + q_y^2 + q_z^2 = \frac{\omega^2}{c_{i,s}^2}, \quad \text{i.e.,} \quad q_y^2 + q_z^2 < \frac{\omega^2}{c_{i,s}^2}, \tag{5}$$

where $c_{i,s}$ is the speed of sound. For large transverse sizes $L_{y,z}=N_{y,z}\,a$, the number of the incoming phonon modes on side i is

$$N_i = \frac{L_y L_z}{4\pi}\sum_{s-1}^{3}\frac{\omega^2}{c_{i,s}^2}, \tag{6}$$

and this leads to the classic low frequency limit[2]

$$\mathcal{T}_{1\to 2} = \frac{\Sigma_s c_{2,s}^{-2}}{\Sigma_s c_{1,s}^{-2} + \Sigma_s c_{2,s}^{-2}}. \tag{7}$$

We note that because of the nonlinear and anisotropic fcc phonon dispersion from the discrete fcc lattice structure, the diffuse phonon transmissivity by Eq. (4) is frequency dependent. Some more simplified models use a single $\langle\mathcal{T}\rangle$ value that is the average over the whole phonon spectrum,[11,12]

$$\langle\mathcal{T}\rangle = \frac{\int\mathcal{T}(\omega)I(\omega,T)d\omega}{\int I(\omega,T)d\omega}, \tag{8}$$

where $I(\omega,T)$ is the incoming phonon energy flux at temperature T. Because $\mathcal{T}(\omega)$ by Eq. (4) varies with frequency, $\langle\mathcal{T}\rangle$ becomes temperature dependent.

Empirically, any phonon scattering process can be treated as partially specular and partially diffuse,[13] which can be quantified by an interface specularity parameter P defined by

$$\mathcal{T} = P\mathcal{T}_{\text{spec}} + (1-P)\mathcal{T}_{\text{diff}}. \tag{9}$$

The specularity varies with interface roughness and must, of course, depend on the incoming phonon modes.

It is possible to precisely solve the scattering problems for well defined large systems. The results of such computations are used herein to validate AMM and DMM, and they can also be directly used in a phonon BTE simulation as boundary conditions. The phonon wave packet simulation tracks the time evolution of a phonon wave packet that initially moves toward a lattice interface or a grain boundary.[14,15] The transmission coefficients are obtained from the division of lattice energy between the two leads after the scattered waves have propagated away from the interface. Although easy to implement, the wave packet method needs to perform one molecular dynamics simulation for each incoming phonon mode, and so the computation would be prohibitively expensive for lattices of large cross sections. For the purpose of elastic scattering calculation, the lattice dynamical approach is more efficient by exploiting the linearity of the system. Fagas *et al.*[16] applied a lattice Green's function formulation to solve the effectively two-dimensional phonon scattering problem between two identical lattice leads, where the otherwise uniform atomic mass is perturbed at the interface. In this paper, we use a similar formulation to solve the elastic phonon scattering problem at a rough interface between two fcc lattice leads, whose phonon dispersion relation mimics the acoustic branches of silicon and germanium. Section II gives the details of the numerical method for solving the scattering problem. The results are shown in Sec. III and are there compared to the specular scattering and diffuse scattering models. Findings are summarized in Sec. IV.

II. GREEN'S FUNCTION FORMULATION

We first solve Green's function for an infinite homogeneous lattice to determine the force needed for activating an incoming phonon mode. Applying this force to the composite lattice whose Green's function we also solve, we obtain the lattice response and extract from it the complex amplitudes

of all scattered phonon waves. In the following subsections, we outline the procedures for solving the phonon scattering problem; the complete details of the general Green's function formalism can be found in Refs. 17 and 18.

We define the ith lattice layer to be the set of $N=2N_yN_z$ atoms that has indexes (i,j,k), where $0\leqslant j<2N_y$, $0\leqslant k<2N_z$, and $j+k\equiv i \pmod 2$. The atoms in each layer are numbered from 1 to N, and we define vector $\mathbf{U}_i$ of length $3N$ to be the atomic displacement of the ith layer. The lattice Hamiltonian can be written in a one-dimensional form

$$H=\frac{1}{2}\sum_i \dot{\mathbf{U}}_i^T\mathbf{M}_i\dot{\mathbf{U}}_i+\frac{1}{2}\sum_{ij}\mathbf{U}_i^T\mathbf{H}_{ij}\mathbf{U}_j, \tag{10}$$

where $\mathbf{M}_i$ is the $3N\times 3N$ diagonal mass matrix and

$$\mathbf{H}_{ij}=\frac{\partial^2 H}{\partial\mathbf{U}_i\partial\mathbf{U}_j} \tag{11}$$

is the interaction matrix between the ith and jth layers. Since only nearest neighbors interact, $\mathbf{H}_{ij}$ is nonzero only for $j=i$ and $j=i\pm 1$.

For elastic scattering at a rough interface, all scattered phonons match the frequency of the incident phonon, but can have any of the transverse wave numbers that are supported by the boundary conditions. The needed Green's function $\mathbf{G}$ to solve this system is equivalent to the solution to the lattice motion activated by an external force acting on one lattice layer. In the frequency domain, the equation for $\mathbf{G}$ is

$$\mathbf{H}_{j-1,j}\mathbf{G}_{ji}+(-\omega^2\mathbf{M}_j+\mathbf{H}_{jj})\mathbf{G}_{ji}+\mathbf{H}_{j,j+1}\mathbf{G}_{j+1,i}=\delta_{ij}\mathbf{I}. \tag{12}$$

For force $\mathbf{F}e^{-i\omega t}$ acting on the ith lattice layer, the atomic response of the jth layer is $\mathbf{U}_j=\mathbf{G}_{ji}\mathbf{F}e^{-i\omega t}$.

A. Green's functions for infinite lattices

For an infinite homogeneous lattice, the lattice Green's function is the superposition of phonon modes at the same frequency ω. All phonon wave numbers lie in the first Brillouin zone, which we choose to be the rectangular box,

$$-\frac{2\pi}{a}\leqslant q_{x,y}<\frac{2\pi}{a},\quad 0\leqslant q_z<\frac{2\pi}{a}. \tag{13}$$

At a real frequency ω, the periodic boundary conditions support $N=2N_yN_z$ transverse wave numbers

$$(q_y,q_z)=\left(\frac{2\pi k_y}{N_y},\frac{2\pi k_z}{N_z}\right) \tag{14}$$

with $-N_y\leqslant k_y<N_y$ and $0\leqslant k_z<N_z$. For each (q_y,q_z), there are six possible q_x with associated polarization vector $\boldsymbol{\xi}$ that satisfy the dispersion relation. Of these, three are right going, with either positive group velocity or positive $\mathrm{Im}(q_x)$, and three are left going. At certain frequencies, a degeneracy yields some solutions with zero x direction group velocity. To avoid the numerical difficulties encountered in such situations, we always add to ω a small positive imaginary part, $i\epsilon\omega$. It ensures that all q_x solutions have nonzero imaginary parts, whose signs are used to identify the the phonon propagating directions. Results are confirmed to be insensitive to our $\epsilon=10^{-4}$ choice. The periodic boundary conditions allow $3N$ right-going phonon modes, which are labeled as $(\mathbf{q}_l,\boldsymbol{\xi}_l)$ with $1\leqslant l\leqslant 3N$; the other $3N$ left-going modes are labeled as $(\mathbf{q}_{[l]},\boldsymbol{\xi}_{[l]})$.

The lth right-going mode introduces an atomic motion on the ith layer that is

$$\boldsymbol{\phi}_{i,l}=\begin{pmatrix}\boldsymbol{\xi}_l e^{i(q_yY_1+q_zZ_1)}\\ \boldsymbol{\xi}_l e^{i(q_yY_2+q_zZ_2)}\\ \vdots\\ \boldsymbol{\xi}_l e^{i(q_yY_N+q_zZ_N)}\end{pmatrix}; \tag{15}$$

the motions $\boldsymbol{\phi}_{i,[l]}$ by the left-going modes are defined similarly. Green's function has the form

$$\mathbf{G}_{ji}^{\infty}=\begin{cases}\displaystyle\sum_{l=1}^{3N}\boldsymbol{\phi}_{j,[l]}e^{iq_{[l]}(j-i)a/2}\mathbf{w}_{i,[l]}^H=\boldsymbol{\Phi}_{|j|}\boldsymbol{\Lambda}_-^{|j-i|}\mathbf{W}_{[i]}, & j\leqslant i\\ \displaystyle\sum_{l=1}^{3N}\boldsymbol{\phi}_{j,l}e^{iq_l(j-i)a/2}\mathbf{w}_{i,l}^H=\boldsymbol{\Phi}_j\boldsymbol{\Lambda}_+^{|j-i|}\mathbf{W}_i, & j\geqslant i,\end{cases} \tag{16}$$

where

$$\boldsymbol{\Phi}_i=(\boldsymbol{\phi}_{i,1},\boldsymbol{\phi}_{i,2},\ldots,\boldsymbol{\phi}_{i,3N}), \tag{17}$$

$$\boldsymbol{\Phi}_{[i]}=(\boldsymbol{\phi}_{i,[1]},\boldsymbol{\phi}_{i,[2]},\ldots,\boldsymbol{\phi}_{i,[3N]}), \tag{18}$$

$$\boldsymbol{\Lambda}_+=\mathrm{diag}(e^{iq_1a/2}\mathbf{I}_3,e^{iq_2a/2}\mathbf{I}_3,\ldots,e^{iq_{3N}a/2}\mathbf{I}_3), \tag{19}$$

$$\boldsymbol{\Lambda}_-=\mathrm{diag}(e^{-iq_{[1]}a/2}\mathbf{I}_3,e^{-iq_{[2]}a/2}\mathbf{I}_3,\ldots,e^{-iq_{[3N]}a/2}\mathbf{I}_3). \tag{20}$$

By construction, Green's function consists of left-going modes for $j\leqslant i$ and of right-going modes for $j>i$. It also automatically satisfies the equation of motion (12) for $j\neq i$. What needs to be solved are the two unknown coefficient matrices $\mathbf{W}_i$ and $\mathbf{W}_{[i]}$.

The unknown matrices $\mathbf{W}_i$ and $\mathbf{W}_{[i]}$ are determined from the continuity condition $\boldsymbol{\Phi}_{[i]}\mathbf{W}_{[i]}=\boldsymbol{\Phi}_i\mathbf{W}_i$, and the governing equation at i,

$$\mathbf{H}_{i,i-1}\boldsymbol{\Phi}_{[i-1]}\boldsymbol{\Lambda}_-\mathbf{W}_{[i]}+(\mathbf{H}_{ii}-\omega^2\mathbf{M}_i)\boldsymbol{\Phi}_i\mathbf{W}_i+\mathbf{H}_{i,i+1}\boldsymbol{\Phi}_{i+1}\boldsymbol{\Lambda}_+\mathbf{W}_i=\mathbf{I}, \tag{21}$$

and the solutions are

$$\boldsymbol{\Phi}_{[i]}\mathbf{W}_{[i]}=\boldsymbol{\Phi}_i\mathbf{W}_i=\boldsymbol{\mathcal{V}}_i^{-1}, \tag{22}$$

where

$$\boldsymbol{\mathcal{V}}_i=\mathbf{H}_{i,i-1}\boldsymbol{\Phi}_{[i-1]}\boldsymbol{\Lambda}_-\boldsymbol{\Phi}_{[i]}^{-1}+(\mathbf{H}_{ii}-\omega^2\mathbf{M}_i)+\mathbf{H}_{i,i+1}\boldsymbol{\Phi}_{i+1}\boldsymbol{\Lambda}_+\boldsymbol{\Phi}_i^{-1}. \tag{23}$$

B. Green's functions for semi-infinite leads

A left lead is a semi-infinite lattice that extends to $x=-\infty$ but has atoms of the (i_0+1)th layer fixed, $\mathbf{U}_{i_0+1}\equiv 0$. Green's function of the left lead, denoted by $\mathbf{G}^L$ is the superposition of Green's function of the infinite lead and left-traveling waves,

$$\mathbf{G}^L_{ji} = \mathbf{G}^\infty_{ji} + \mathbf{\Phi}_{[j]}\mathbf{\Lambda}_-^{|j-(i_0+1)|}\tilde{\mathbf{W}}, \quad i,j \leqslant i_0. \tag{24}$$

The coefficient matrix $\tilde{\mathbf{W}}$ is determined by the boundary condition $\mathbf{G}^L_{i_0+1,i}=0$, which gives

$$\tilde{\mathbf{W}} = -\mathbf{\Phi}^{-1}_{[i_0+1]}\mathbf{G}^\infty_{i_0+1,i}. \tag{25}$$

The surface Green's function is

$$\mathbf{g}_L = \mathbf{G}^L_{i_0 i_0} = \mathbf{\Phi}_{[i_0]}\mathbf{W}_L, \tag{26}$$

where

$$\mathbf{W}_L = \mathbf{W}_{[i_0]} - \mathbf{\Lambda}_-\mathbf{\Phi}^{-1}_{[i_0+1]}\mathbf{\Phi}_{i_0+1}\mathbf{\Lambda}_+\mathbf{W}_{i_0}. \tag{27}$$

Similarly, for a right lead that extends to $x=+\infty$ and has boundary condition $\mathbf{U}_{i_0-1}\equiv 0$, its surface Green's function is

$$\mathbf{g}_R = \mathbf{G}^R_{i_0 i_0} = \mathbf{\Phi}_{i_0}\mathbf{W}_R, \tag{28}$$

where

$$\mathbf{W}_R = \mathbf{W}_{i_0} - \mathbf{\Lambda}_+\mathbf{\Phi}^{-1}_{i_0-1}\mathbf{\Phi}_{[i_0-1]}\mathbf{\Lambda}_-\mathbf{W}_{[i_0]}. \tag{29}$$

C. Green's function of the coupled system

The composite lattice consists of the left lead $i<0$, the interface region $0\leqslant i<2N_x$, and the right lead $i\geqslant 2N_x$. To solve the scattering problem, it suffices to know the surface Green's function

$$\mathcal{G} = \begin{pmatrix} \mathcal{G}_{LL} & \mathcal{G}_{LR} \\ \mathcal{G}_{RL} & \mathcal{G}_{RR} \end{pmatrix}, \tag{30}$$

which represents the interaction between the left lead surface [the (-1)th lattice layer] and the right lead surface (the $2N_x$th layer). The $\mathcal{G}$ is determined via Dyson's equation

$$\mathcal{G} = \mathcal{G}^{(0)} - \mathcal{G}^{(0)}\mathcal{H}'\mathcal{G}, \tag{31}$$

which gives the solution

$$\mathcal{G} = (\mathcal{G}^{(0)-1} + \mathcal{H}')^{-1}, \tag{32}$$

Here,

$$\mathcal{G}^{(0)} = \begin{pmatrix} \mathbf{g}_L & \mathbf{0} \\ \mathbf{0} & \mathbf{g}_R \end{pmatrix} \tag{33}$$

is Green's function of the two uncoupled semi-infinite leads, and

$$\mathcal{H}' = \begin{pmatrix} \mathcal{H}'_{LL} & \mathcal{H}'_{LR} \\ \mathcal{H}'_{RL} & \mathcal{H}'_{RR} \end{pmatrix} \tag{34}$$

is the effective Hamiltonian connecting the two lead surfaces at the interface. The matrix $\mathcal{H}'$ can be calculated from a recursive Green's function formulation.[18,19]

D. Transmission and reflection coefficients

Let an incoming phonon wave from $x=-\infty$ be one of the $3N$ right-going modes satisfying the dispersion relation. If the lattice vibration of the incoming mode is $\boldsymbol{\psi}^{(i)}$, we need a surface force of amplitude $\mathbf{F}=\mathcal{V}_{-1}\boldsymbol{\psi}^{(i)}$ acting on the lead surface to activate the incoming wave. The lattice motion on the left lead surface due to the reflected wave is $\boldsymbol{\psi}^{(r)}=\mathcal{G}_{LL}\mathbf{F}-\boldsymbol{\psi}^{(i)}$, and is $\boldsymbol{\psi}^{(t)}=\mathcal{G}_{RL}\mathbf{F}$ on the right lead surface by the transmitted wave. The transmission and reflection coefficients are

$$\mathcal{T} = \frac{I^{(t)}}{I^{(i)}}, \quad \mathcal{R} = \frac{I^{(r)}}{I^{(i)}}, \tag{35}$$

where the I factors represent the energy flow associated with the incoming (i), transmitted (t), and reflected (r) waves.

Since each of the incoming, reflected, and transmitted waves is composed of phonon modes traveling in the same direction, its energy flows can be easily determined by a phonon mode decomposition. Let $\boldsymbol{\psi}_i$ be the displacement of the ith layer due to one of the three waves. Supposing $\boldsymbol{\psi}$'s component phonon modes are all right moving, its mode decomposition can then be written as

$$\boldsymbol{\psi}_i = \mathbf{\Phi}_i\hat{\boldsymbol{\psi}}_i = \sum_{l=1}^{3N}\hat{\psi}_{i,l}\boldsymbol{\phi}_{i,l}, \tag{36}$$

where the phonon amplitude vector is $\hat{\boldsymbol{\psi}}_i=\mathbf{\Phi}_i^{-1}\boldsymbol{\psi}_i$. Hence the energy flow induced is

$$I = \sum_{l=1}^{3N} Mc_l|\hat{\psi}_{i,l}|^2, \tag{37}$$

where c_l is the group velocity of the lth phonon mode.

For validation, we computed the phonon scattering at an atomically smooth interface with 8×8 cells in transverse directions, and compared the result to the specular scattering calculation.[8,9] The transmission coefficients computed by the two methods differ by less than 0.1% for all incoming modes. The difference is from the small imaginary part of ω in Green's function formula.

III. RESULTS

A. Interface generation

The interfaces we consider are constructed with an approximately Gaussian two-point height correlation,

$$\langle h(\mathbf{y}_1)h(\mathbf{y}_2)\rangle \approx \sigma^2\sum_{\mathbf{b}}\exp\left(-\frac{|\mathbf{y}_1-\mathbf{y}_2-\mathbf{b}|^2}{\lambda^2}\right), \tag{38}$$

where $\mathbf{b}=(n_yL_y, n_zL_z)$. The surface roughness is quantified by σ the average height and λ the correlation distance. Numerically, the discrete values of h are generated by a Fourier transform on a $2N_y\times 2N_z$ uniform Cartesian mesh. The discrete values of h are

$$h_{j_yj_z} = \sum_{k_y=-N_y}^{N_y-1}\sum_{k_z=-N_z}^{N_z-1}\hat{h}_{k_yk_z}\exp\left(\mathrm{i}\frac{\pi j_yk_y}{N_y}\right)\exp\left(\mathrm{i}\frac{\pi j_zk_z}{N_z}\right), \tag{39}$$

where each Fourier coefficient $\hat{h}_{k_yk_z}$ is

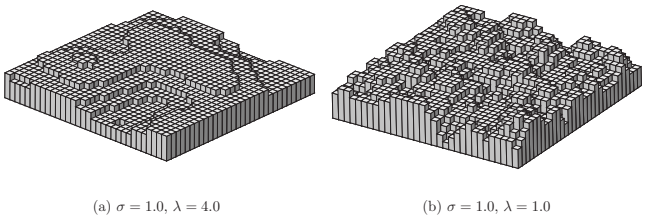

(a) $\sigma = 1.0$, $\lambda = 4.0$ (b) $\sigma = 1.0$, $\lambda = 1.0$

FIG. 2. Two randomly generated interfaces. The discreet value of the interface height is defined as the biggest integer that is less than $h_{j_y j_z}$ for every (j_y, j_z).

$$\hat{h}_{k_y k_z} = \sqrt{\frac{\pi\sigma^2\lambda^2}{L_y L_z}} \exp\left(-\frac{|\mathbf{q}_{yz}|^2\lambda^2}{8}\right)\exp(\mathrm{i}\boldsymbol{\phi}_{k_y k_z})$$

$$\text{with } \mathbf{q}_{yz} = \left(\frac{2\pi k_y}{L_y}, \frac{2\pi k_z}{L_z}\right). \tag{40}$$

The Fourier coefficients $\hat{h}_{k_y k_z}$ are assigned with random phase angles $\phi_{k_y k_z}$, but with the symmetry condition $\hat{h}_{k_y k_z} = \hat{h}^*_{-k_y,-k_z}$ respected. Two example interfaces of different correlation lengths are visualized in Fig. 2. For each (σ, λ) pair studied, 16 Gaussian interfaces are generated, and their scattering computation results are averaged for presentation here.

B. Interface specularity

The interface specularity P for incoming phonons of normal incidence from the left Si lead is plotted in Fig. 3. The wave numbers are in the low to medium range $q_x/(2\pi) < 0.4$. Three sets of roughness parameters are studied, with $(\sigma, \lambda) = (1.0, 1.0)$, (1.5, 1.0), and (1.5, 4.0), respectively. Not surprisingly, P decays with increasing wave number, and it also decreases with increasing σ, the magnitude of variation in surface height. Figure 3 also shows the effect of the phonon polarization. For the $\lambda = 4.0$, case where the interface is smooth (see Fig. 2), the difference in the specularities of the two polarizations is insignificant. For the two rougher interfaces with $\lambda = 1.0$, we observe significant separations in P between the longitudinal and the transverse modes, with the transverse mode consistently having higher

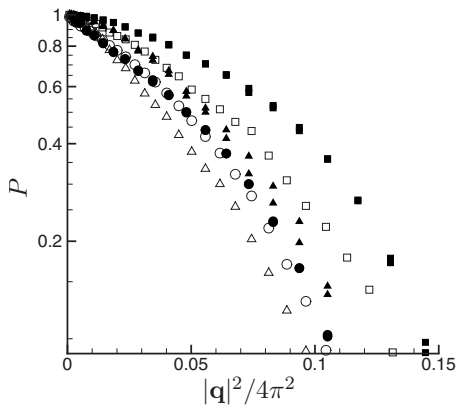

FIG. 3. Interface specularity defined in Eq. (9) for incoming modes of normal incidence for roughness parameters: $\sigma = 1.0$ and $\lambda = 1.0$ □ (■); $\sigma = 1.5$ and $\lambda = 1.0$ △ (▲); and $\sigma = 1.5$ and $\lambda = 4.0$ for ○ (●). Hollow symbols are for incoming phonons of longitudinal modes, and solid symbols are for transverse modes.

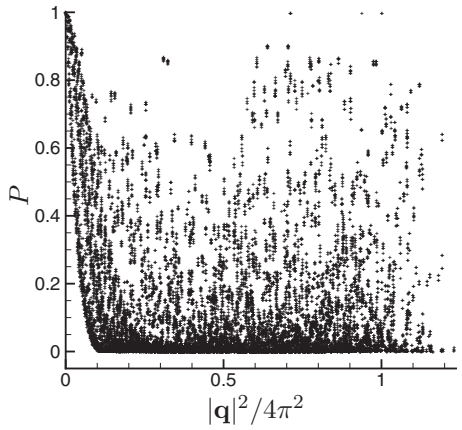

FIG. 4. Specularity of all incident phonons from the left (Si) lead.

specularity. These results suggest that at low wave numbers, the specular transmission of the shear waves is less disrupted by the rough interface than compressive waves.

Figure 4 shows the scattering specularity for all incoming modes. The roughness parameters are $\sigma = 1.5$ and $\lambda = 1.0$. Although a single functional relation between P and $|\mathbf{q}|$ is not expected, the trend of P decreasing with $|\mathbf{q}|$ is obvious. For $|\mathbf{q}| > 0.4\pi$, 95% incoming modes have $P < 0.2$, and scattering is predominantly diffuse. For the 16×16 lattice cross section, the artifact of the finite size effect is apparent in places, but the general trends are clear. For example, the incoming phonons whose frequency approaches its upper limit exhibit abnormally high specularity, since there are only limited number of possible scattered phonon modes with the discrete transverse wave numbers.

The specularity averaged at each frequency ω is plotted in Figs. 5 and 6. In Fig. 5, the interfaces have the same $\lambda = 1.0$ but different $\sigma = 0.5$, 1.0, and 1.5. For each of the three interfaces, P decreases with ω. As discussed before, the abnormal increase in P as ω approaches its maximum is an artifact due to the finite domain size. The curves of different σ are well separated; interfaces with bigger σ are consistently less specular at all frequencies. The plots in Fig. 6 are from the three interfaces with $\sigma = 1.5$ and $\lambda = 1.0$, 2.0, and 4.0. The correlation length λ has a minor effect on P, as manifested by the smaller separations among the P-ω curves. Indeed, the roughest interface with $\lambda = 1.0$ has the highest specularity value, especially at $\omega < 1.0$. Our explanation for this is that for low frequency (thus small wave number) incoming phonons, the $\lambda = 4$ interface is locally smooth so the scattering is predominantly specular. However the local interface normal is different from the x axis, and so the locally specular scatterings still result in a globally diffuse scattering.

C. Transmissivity and thermal boundary resistance

The average transmission coefficient is shown in Fig. 7, and is compared to those by the specular scattering computation and by the DMM. The interfaces used are the same as those in Fig. 5. The $\mathcal{T}$ values computed by these different approaches have similar trends versus ω. Interfaces with dif-

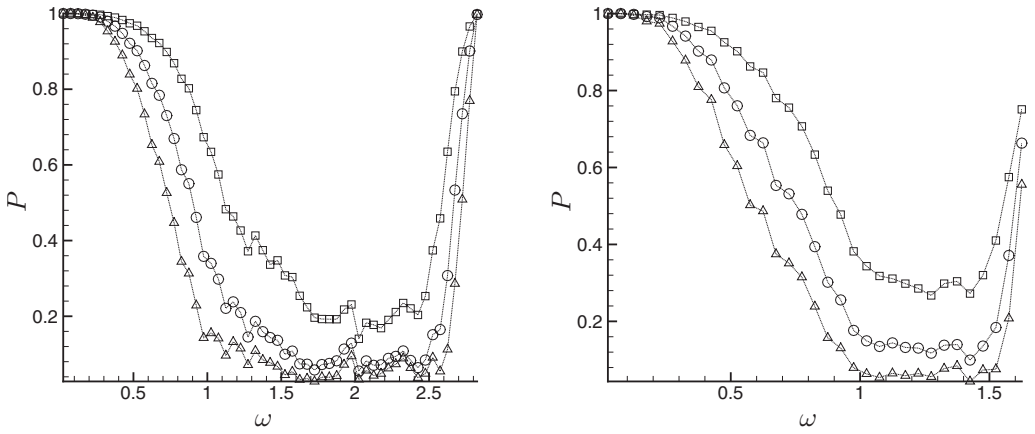

(a) Incoming from left (b) Incoming from right

FIG. 5. Interface specularity with $\lambda=1.0$ and (□) $\sigma=0.5$, (○) $\sigma=1.0$, and (△) $\sigma=1.5$.

ferent σ do not have significant difference in $\mathcal{T}$, even though they differ significantly in the scattering specularity. We compute the normalized $\mathcal{T}_{\text{spec}}$ and $\mathcal{T}_{\text{diff}}$,

$$\tilde{\mathcal{T}}_{\text{spec}}=\frac{\mathcal{T}_{\text{spec}}}{\mathcal{T}_{\text{spec}}+\mathcal{R}_{\text{spec}}},\quad \tilde{\mathcal{T}}_{\text{diff}}=\frac{\mathcal{T}_{\text{diff}}}{\mathcal{T}_{\text{diff}}+\mathcal{R}_{\text{diff}}}. \tag{41}$$

These measure the relative contribution to phonon transmission via the specular and diffuse mechanism, and are compared to the predictions by the specular scattering and diffuse scattering models in Fig. 8. Agreement is good with the specular scattering model at low frequency ($\omega<1$), and with the diffuse scattering model at higher frequency; the relative difference is within 20% except near $\omega=1.5$. Again σ has little effect on both $\tilde{\mathcal{T}}_{\text{spec}}$ and $\tilde{\mathcal{T}}_{\text{diff}}$. The $\mathcal{T}$ computed using interfaces of different λ values have similar trends, so they are not included here.

The thermal boundary resistance (or Kapitza resistance) κ results from the phonon scattering at the interface,

$$\kappa=\frac{\Delta T}{\Delta I}=\frac{T_1-T_2}{I_{1\to 2}-I_{2\to 1}}, \tag{42}$$

where ΔI is the net energy flow per unit area across the interface, and ΔT is the temperature jump across the interface. The incoming energy flow from the left is

$$I_{1\to 2}=\frac{1}{(2\pi)^3}\int_{\mathbf{q}_1}\sum_s \hbar\omega(\mathbf{q}_1,s)c_x(\mathbf{q}_1,s)\mathcal{T}_{1\to 2}(\mathbf{q}_1,s)\times n(\omega,T_1^{(i)})d\mathbf{q}_1, \tag{43}$$

where the integration is over all incoming phonons from the left ($c_x>0$), n is the phonon occupation number, and $T^{(i)}$ is the incoming phonon temperature. We have assumed that the incoming phonon distribution is not disturbed by the interface scattering. Using the fact that $\Delta I=0$ when $\Delta T^{(i)}=0$, we have the following formula for the thermal boundary conductance κ^{-1}:

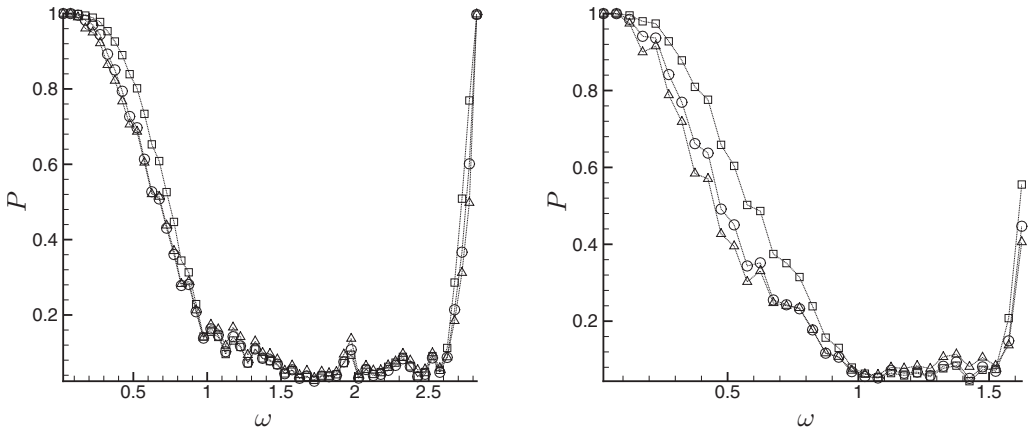

(a) Incoming from left (b) Incoming from right

FIG. 6. Interface specularity with $\sigma=1.5$ and (□) $\lambda=1.0$, (○) $\lambda=2.0$, and (△) $\lambda=4.0$.

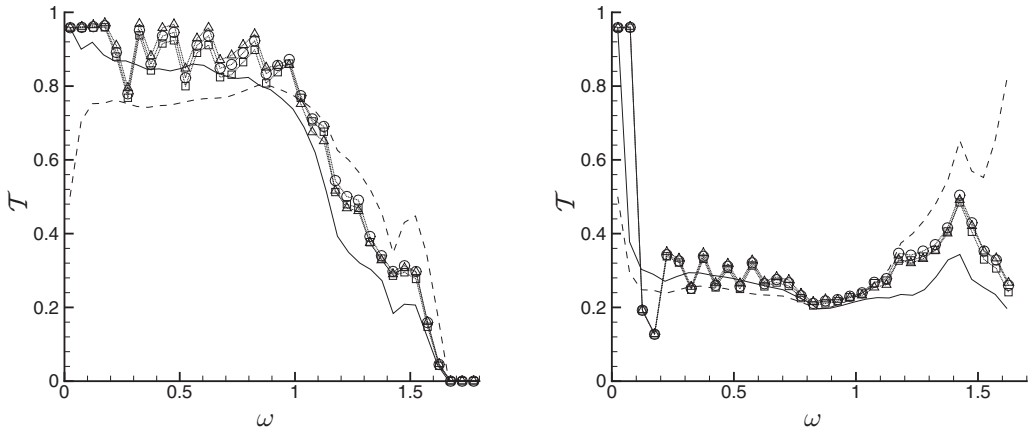

(a) Incoming from left (b) Incoming from right

FIG. 7. Transmission coefficient with $\lambda=1.0$ and (□) $\sigma=0.5$, (○) $\sigma=1.0$, and (△) $\sigma=1.5$. (—) is the specular scattering calculation and (----) is by DMM.

$$\kappa^{-1} = \frac{\Delta I}{\Delta T^{(i)}} = \frac{1}{(2\pi)^3}\int_{\mathbf{q}_1}\sum_s \hbar\omega(\mathbf{q}_1,s)c_x(\mathbf{q}_1,s)\mathcal{T}_{1\to 2}(\mathbf{q}_1,s)\frac{\partial n}{\partial T}d\mathbf{q}_1 \tag{44}$$

for small temperature jump.

An alternative definition of thermal boundary resistance that is more relevant to experimental measurements uses the jump in equilibrium phonon temperature $T^{(e)}$ instead of the incoming phonon temperature $T^{(i)}$.[11,12] The equilibrium phonon temperature is determined by the total phonon energy density, which is the sum of contributions from the incoming, reflected, and transmitted phonons. Without solving the full phonon BTE, we can calculate $T^{(e)}$ approximately assuming the following:

- The scattered phonons (reflected and transmitted) reach thermal equilibrium through phonon collisions. These collisions are assumed to be N-processes, and thus do not change the total back scattering energy flow. Therefore, the temperature of scattered phonons, $T^{(s)}$, can be computed from their total energy flow.
- For small $\Delta T^{(i)}$, the equilibrium phonon temperature is the average of those of the incoming and scattered phonons, i.e., $T^{(e)}=(T^{(i)}+T^{(s)})/2$.

The scattered phonon temperatures can then be calculated by

$$(T_1^{(s)} - T_2^{(i)})\int_{\mathbf{q}_1}\sum_s \hbar\omega(\mathbf{q}_1,s)c_x(\mathbf{q}_1,s)\frac{\partial n}{\partial T}d\mathbf{q}_1 = (T_1^{(i)} - T_2^{(i)})\int_{\mathbf{q}_1}\sum_s \hbar\omega(\mathbf{q}_1,s)(1-\mathcal{T}_{1\to 2})c_x(\mathbf{q}_1,s)\frac{\partial n}{\partial T}d\mathbf{q}_1, \tag{45}$$

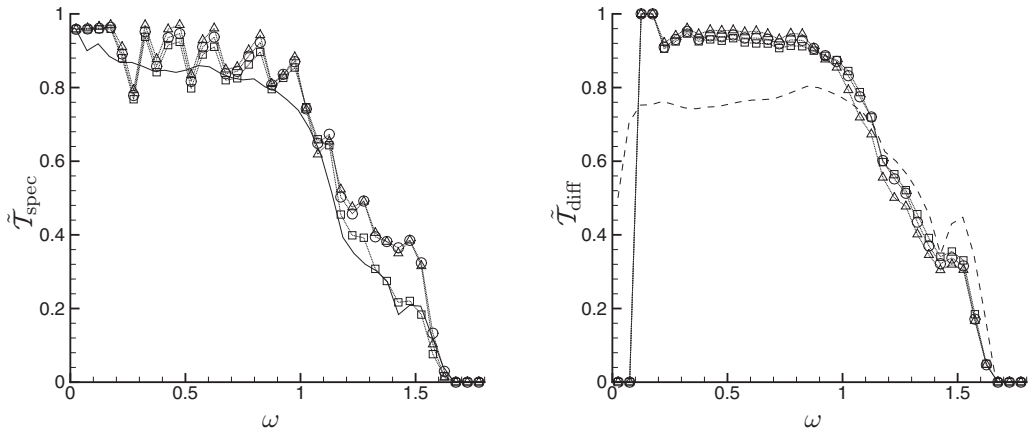

(a) (b)

FIG. 8. Normalized $\tilde{\mathcal{T}}_{\text{spec}}$ and $\tilde{\mathcal{T}}_{\text{diff}}$ with $\lambda=1.0$ and (□) $\sigma=0.5$, (○) $\sigma=1.0$, and (▲) $\sigma=1.5$. (—) is by the specular scattering calculation and (----) is by DMM. Incoming phonons are from the lead lead.

TABLE I. Kapitza conductance at 300 K as defined by Eq. (42) based on the jumps in the incoming phonon temperature $T^{(i)}$ and the equilibrium phonon temperature $T^{(e)}$.

	$\kappa^{-1}(10^8\ \mathrm{W\ K^{-1}\ m^{-2}})$	
	$\Delta I/\Delta T^{(i)}$	$\Delta I/\Delta T^{(e)}$
Specular scattering	1.11	1.38
Diffuse scattering	1.56	2.15
Green's function results	1.35 ± 0.05	1.78 ± 0.06
Specular scattering (diamond structure)	3.26	4.69

$$(T_2^{(s)} - T_1^{(i)}) \int_{\mathbf{q}_2} \sum_s \hbar\omega(\mathbf{q}_2,s) c_x(\mathbf{q}_2,s) \frac{\partial n}{\partial T} d\mathbf{q}_2 = (T_2^{(i)} - T_1^{(i)}) \int_{\mathbf{q}_2} \sum_s \hbar\omega(\mathbf{q}_2,s)(1 - \mathcal{T}_{2\to 1}) c_x(\mathbf{q}_2,s) \frac{\partial n}{\partial T} d\mathbf{q}_2, \tag{46}$$

where all the integrals are over incoming phonon modes. Obviously, the discontinuity in the apparent temperature is less than that in the incoming phonon temperature, i.e., $0 \leqslant \Delta T^{(e)}/\Delta T^{(i)} \leqslant 1$. The ratio $\Delta T^{(e)}/\Delta T^{(i)}$ decreases with increasing phonon transmissivity. In the trivial case where the two lattice leads have identical atoms, all incoming phonons have unit transmissivity ($\mathcal{T} \equiv 1$). Consequently, the two leads have the same equilibrium temperature $T_1^{(e)} = T_2^{(e)} = (T_1^{(i)} + T_2^{(i)})/2$, and the Kapitza resistance is zero.

The computed κ^{-1} at 300 K are listed in Table I. Since the transmission coefficients are insensitive to the surface roughness, the overall Kapitza conductance is also largely independent of the surface roughness. The κ^{-1} based on $\Delta T^{(i)}$ are in the range of 1.35 ± 0.05 W K^{-1} m^{-2} for the interfaces with various roughness parameters in Figs. 5 and 6. For the alternative definition $\kappa^{-1} = \Delta I/\Delta T^{(e)}$, the values are augmented by 30% to 1.78 ± 0.06 W K^{-1} m^{-2}. These κ^{-1} values lie between the predictions by the specular scattering model and the diffuse scattering model that are also listed in Table I. For the two lattice leads considered here that have very different acoustic properties, the diffuse scattering enhances the phonon transmissivity, especially at high frequencies, resulting in a higher thermal boundary conductance compared to the perfectly specular interface.

Also listed in Table I are the κ^{-1} values by the specular scattering calculation using the true diamond structure, which is almost three times of that by the simple fcc model. The discrepancy can be explained by the frequency histograms of κ^{-1} shown in Fig. 9. The fcc and diamond lattice models agree well at frequencies less than 4 THz, but the fcc model seriously underestimates the contribution to κ^{-1} from high frequency phonons. The reasons are (1) the flattening of the fcc phonon dispersion curves near the Brillouin zone boundary and the resulting smaller group velocities and (2) the missing of acoustic and optical phonon mode conversion.[9]

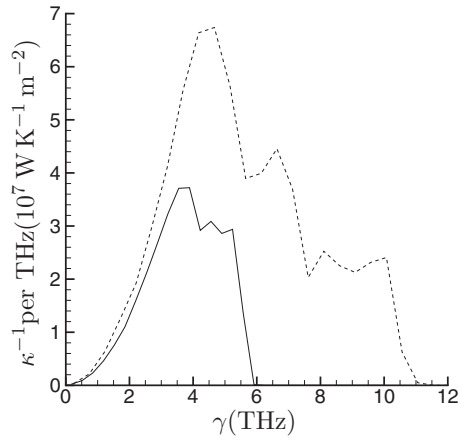

FIG. 9. Histogram of Kapitza conductance at 300 K: (—) using an fcc lattice model and (----) using a diamond structure and specular model. The incoming phonons are from the left (Si) lattice lead.

IV. CONCLUSION

We have used a lattice Green's function method to calculate the elastic phonon scattering at a rough interface between two semi-infinite fcc lattice leads, whose phonon dispersions approximates those of the bulk Si and Ge. The roughness of the interface is quantified by the σ the magnitude of the interface height variation, and λ the correlation length. The average interface specularity during the scattering process shows a strong influence from σ, while the dependence on λ is weak. For normal incidences, the transverse incoming phonons are shown to have larger specularity than the longitudinal ones of the same wave number, especially for interface of small λ.

The normalized phonon transmission coefficients agree well with the specular scattering model at low frequency, and with the diffuse scattering model at higher frequencies. In contrast to the interface specularity, the overall transmission coefficients do not have significant dependence on either σ or λ. Consequently, the thermal boundary resistance in the linear limit is insensitive to those roughness parameters. When the temperature jump across the interface is finite, a full phonon BTE simulation would be necessary to investigate the impact of the phonon spectrum that varies with the interface roughness.

ACKNOWLEDGMENTS

We gratefully acknowledge the support from the National Science Foundation.

[1] P. L. Kapitza, J. Phys. (USSR) **4**, 181 (1941).
[2] E. T. Swartz and R. O. Pohl, Rev. Mod. Phys. **61**, 605 (1989).
[3] S. Mazumder and A. Majumdar, J. Heat Transfer **123**, 749 (2001).
[4] R. G. Yang and G. Chen, Phys. Rev. B **69**, 195316 (2004).
[5] T. Zeng and G. Chen, J. Heat Transfer **123**, 340 (2001).
[6] S. Tamura, Y. Tanaka, and H. J. Maris, Phys. Rev. B **60**, 2627 (1999).
[7] W. A. Little, Can. J. Phys. **37**, 334 (1959).
[8] D. A. Young and H. J. Maris, Phys. Rev. B **40**, 3685 (1989).
[9] H. Zhao and J. B. Freund, J. Appl. Phys. **97**, 024903 (2005).
[10] P. Debye, Ann. Phys. **39**, 789 (1912).
[11] G. Cheng, *Nanoscale Energy Transport and Conversion* (Oxford University Press, New York, 2005).
[12] C. Dames and G. Chen, J. Appl. Phys. **95**, 682 (2004).
[13] G. Chen, Phys. Rev. B **57**, 14958 (1998).

[14]P. K. Schelling, S. R. Phillpot, and P. Keblinkski, Appl. Phys. Lett. **80**, 2484 (2003).
[15]P. K. Schelling, S. R. Phillpot, and P. Keblinski, J. Appl. Phys. **95**, 6082 (2004).
[16]G. Fagas, A. G. Kozorezov, C. J. Lambert, and J. K. Wigmore, Phys. Rev. B **60**, 6459 (1999).
[17]S. Sanvito, "Giant magnetoresistance and quantum transport in magnetic hybrid nanostructures," Ph.D. thesis, Lancaster University, 1999.
[18]S. Sanvito, C. J. Lambert, J. H. Jefferson, and A. M. Bratkovsky, Phys. Rev. B **59**, 11936 (1999).
[19]C. J. Lambert, V. C. Hui, and S. J. Robinson, J. Phys.: Condens. Matter **5**, 4187 (1993).